

Cell Reports, Volume 22

Supplemental Information

**Energy Scarcity Promotes a Brain-wide Sleep State
Modulated by Insulin Signaling in *C. elegans***

Susanne Skora, Fanny Mende, and Manuel Zimmer

Supplemental information

This PDF contains:

Supplemental figures S1-S7
Supplemental figure legends
Supplemental table S1
Supplemental experimental procedures
Supplemental references

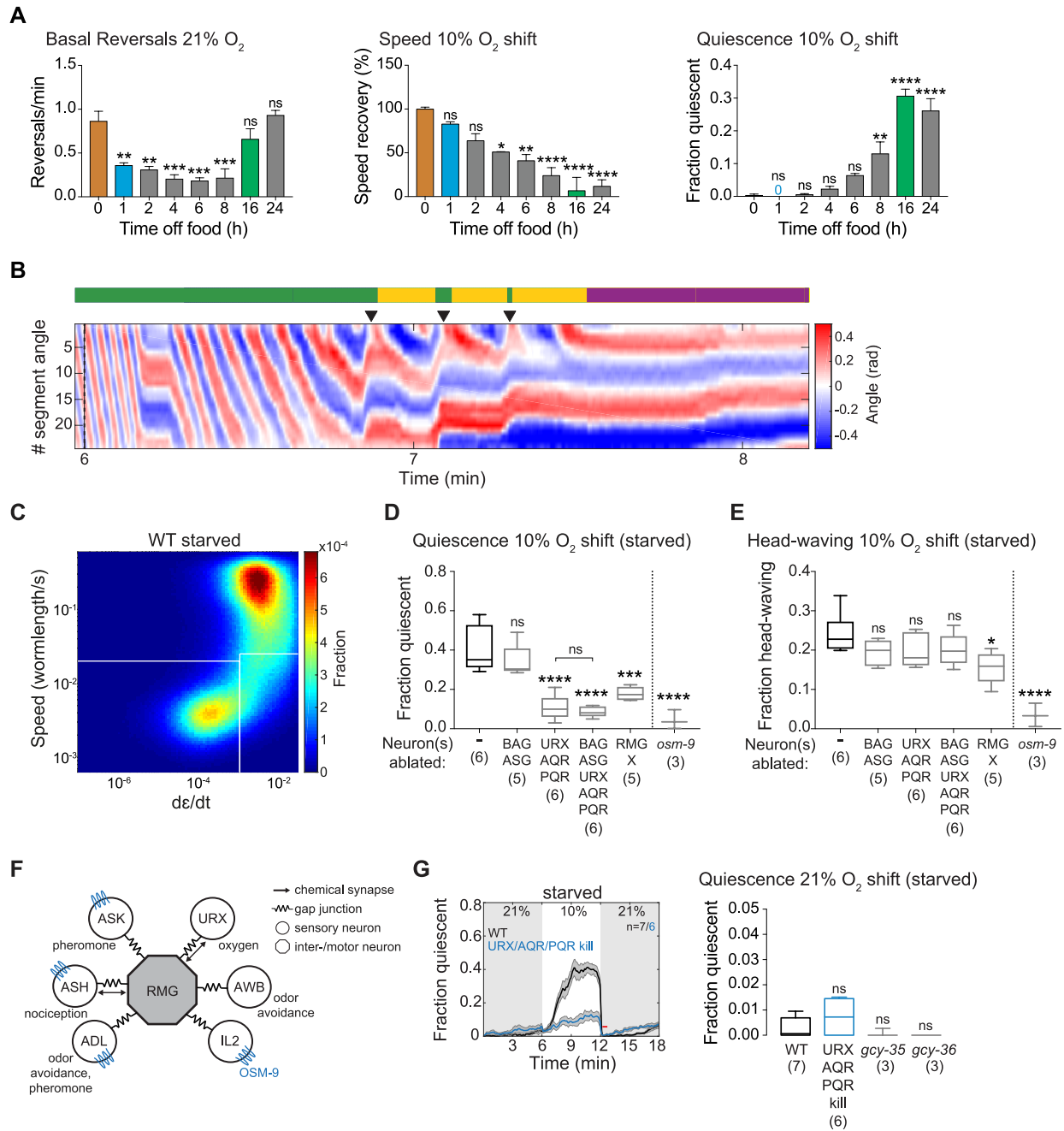


Figure S1. Food deprivation causes a gradual change in O₂-related behaviors and quiescence is under control of sensory circuits. Related to Figure 1.

(A) Quantification of basal reversal rate, speed recovery following O₂ downshift and O₂ downshift-induced quiescence, upon increasing time off food. Basal reversal rate was quantified during interval labelled with black bar in Figure 1A, speed recovery and quiescence as described for Figures 1B and 1C. 0 h off food indicates well-fed. Bars show mean \pm SEM. Bar colors match colors in Figure 1. Time points were compared to the well-fed condition using one-way ANOVA with Dunnett's correction (**** $p < 0.0001$, *** $p \leq 0.001$, ** $p \leq 0.01$, * $p = 0.0106$, ns $p > 0.05$). Number of experiments (n) used: n = 3, except 8 h and 16 h time points for which n = 4 (~100 animals each).

(B) Body posture kymograph of 24 intersegment angles from head (1) to tail (24) for the worm shown in Movie S1. O₂ downshift starts at 6 min into the recording (dotted black line). Colored line above kymograph indicates behavioral state according to color scheme used in Figure 1G (green: active, yellow: head-waving, purple: quiescent). Black arrowheads indicate reversals.

(C) 2D fractional density distribution (log-log scale) of speed vs. derivative of eccentricity ($d\epsilon/dt$) of WT starved animals from all experiments of the type shown in Figure 1C (n=28) and the experiments shown in Figures 1E and 1F (n=4 each), including all O₂ concentration periods. White lines indicate the thresholds used to identify behavioral states (quiescent: < 0.00107 ($d\epsilon/dt$) and < 0.02 (speed); head-waving: > 0.00107 ($d\epsilon/dt$) and < 0.025 (speed)).

(D and E) Effect of neuronal ablations and sensory signaling-defective *osm-9* mutants on quiescence **(D)** and head-waving **(E)**. Quantification intervals as in Figures 1C and 1D. The X denoted with RMG ablation strain signifies ablation of an additional unknown neuron, see note with methods. Boxplots display median, interquartile range and min to max whiskers. All strains were compared to WT and additional comparisons were made as indicated, using one-way ANOVA with Sidak's correction (**** $p < 0.0001$, *** $p = 0.0002$, * $p = 0.0112$, ns $p > 0.05$). Number of experiments (n) indicated below each genotype.

(F) Illustration of hub and spoke circuit diagram showing RMG and its gap junction sensory neuron partners. OSM-9-expressing neurons indicated in blue, according to Colbert et al., 1997.

(G) Left: Population means (\pm SEM) of fraction quiescent under O_2 stimulation as indicated for starved WT (black) and URX/AQR/PQR-ablated (blue) animals. Right: Quantification during period indicated by red bar in left panel. Quantification additionally shows animals deficient in the guanylate cyclases *gcy-35* and *gcy-36*, which are required for O_2 sensation. Significance against WT determined using one-way ANOVA with Dunnett's correction (ns $p > 0.05$). Boxplots show median, interquartile range and min to max whiskers. Number of experiments (n) indicated below each boxplot. Experiments of URX/AQR/PQR cell kill are the same as those in Figures S1D and S1E.

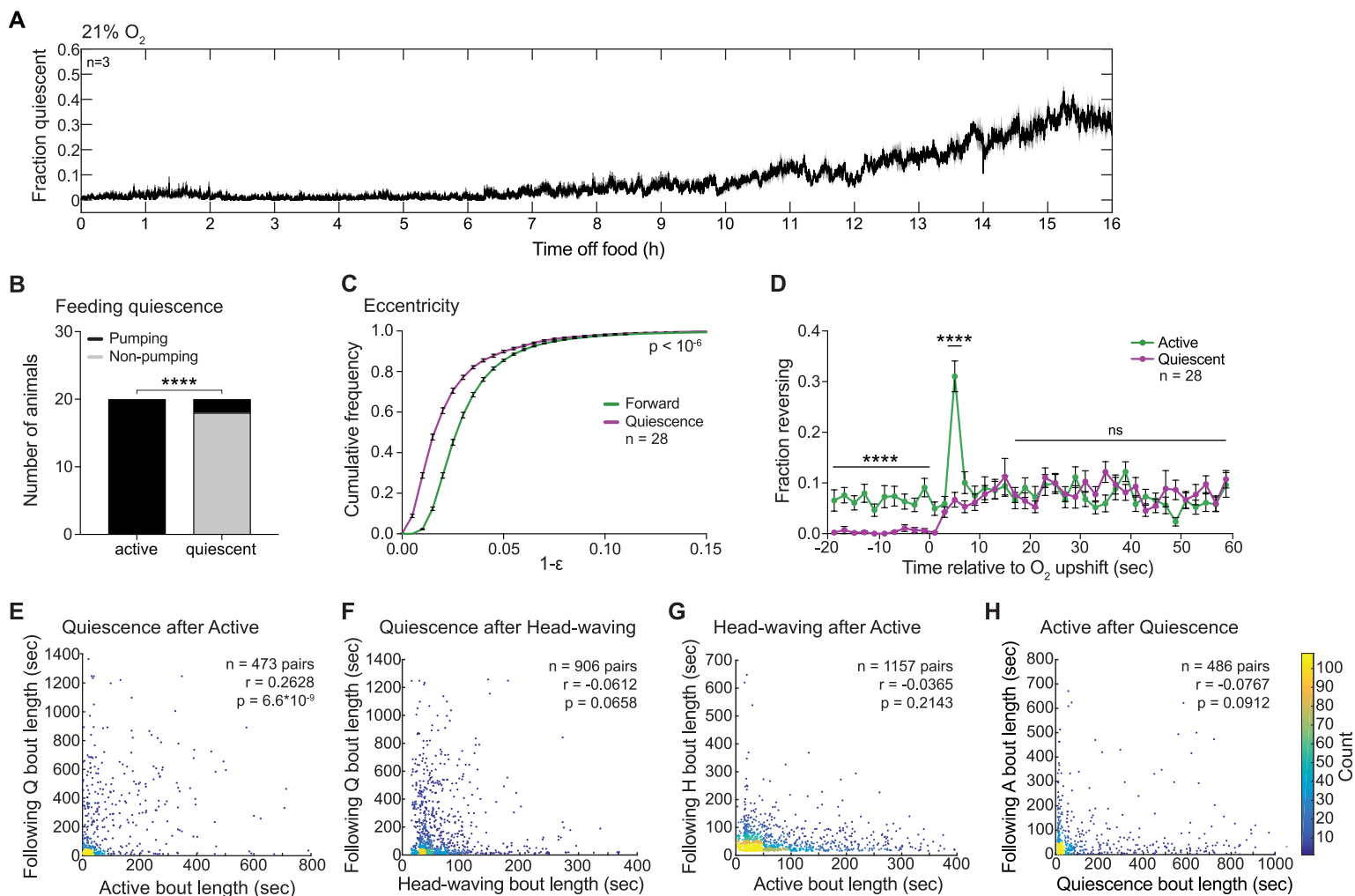


Figure S2. Starvation quiescence is a behavioral sleep-like state. Related to Figure 1.

(A) Population mean (\pm SEM) of fraction quiescent during long-term, undisturbed recording of WT worms at constant 21% O₂. Number of experiments (n) indicated (~100 animals each).

(B) Number of active and quiescent starved WT animals exhibiting pumping versus non-pumping behavior during a 60 sec observation period. Total number of pumps observed in quiescent worms = 3, also see methods. Number of animals (n) = 20 for each active and quiescent. Fisher's exact test (**** p < 0.0001).

(C) Mean (\pm SEM) cumulative fractional distributions of shape factor 1-eccentricity (ϵ) during fast forward movement (> 0.1 mm/sec) versus quiescence from O₂ shift experiments in WT starved animals as in Figure 1C. P-value indicates chance of obtaining an equal or larger difference between the distributions after random shuffling, see methods. Number of experiments (n) indicated.

(D) Mean (\pm SEM) fraction of WT starved animals reversing, both pre and post O₂ upshift. Animals have either been active (green) or quiescent (purple) for 2 min prior to O₂ upshift. Number of experiments (n) indicated. Significance calculated for the time intervals indicated with black lines, using Mann-Whitney test (**** p < 0.0001, ns p = 0.1114).

(E-H) Scatter plots of quiescence (Q) bout length versus preceding active (A) bout length (E), quiescence (Q) bout length versus preceding head-waving bout length (F), head-waving (H) bout length versus preceding active bout length (G), and active (A) bout length versus preceding quiescence bout length (H). Data are taken from experiments shown in Figure 1F at constant 10% O₂, also see methods. n = number of successive bout pairs. Axes are cropped to aid visualization. Color indicates density of data points according to color bar on the right. r = Spearman correlation coefficient. The p-values are approximated by random permutations.

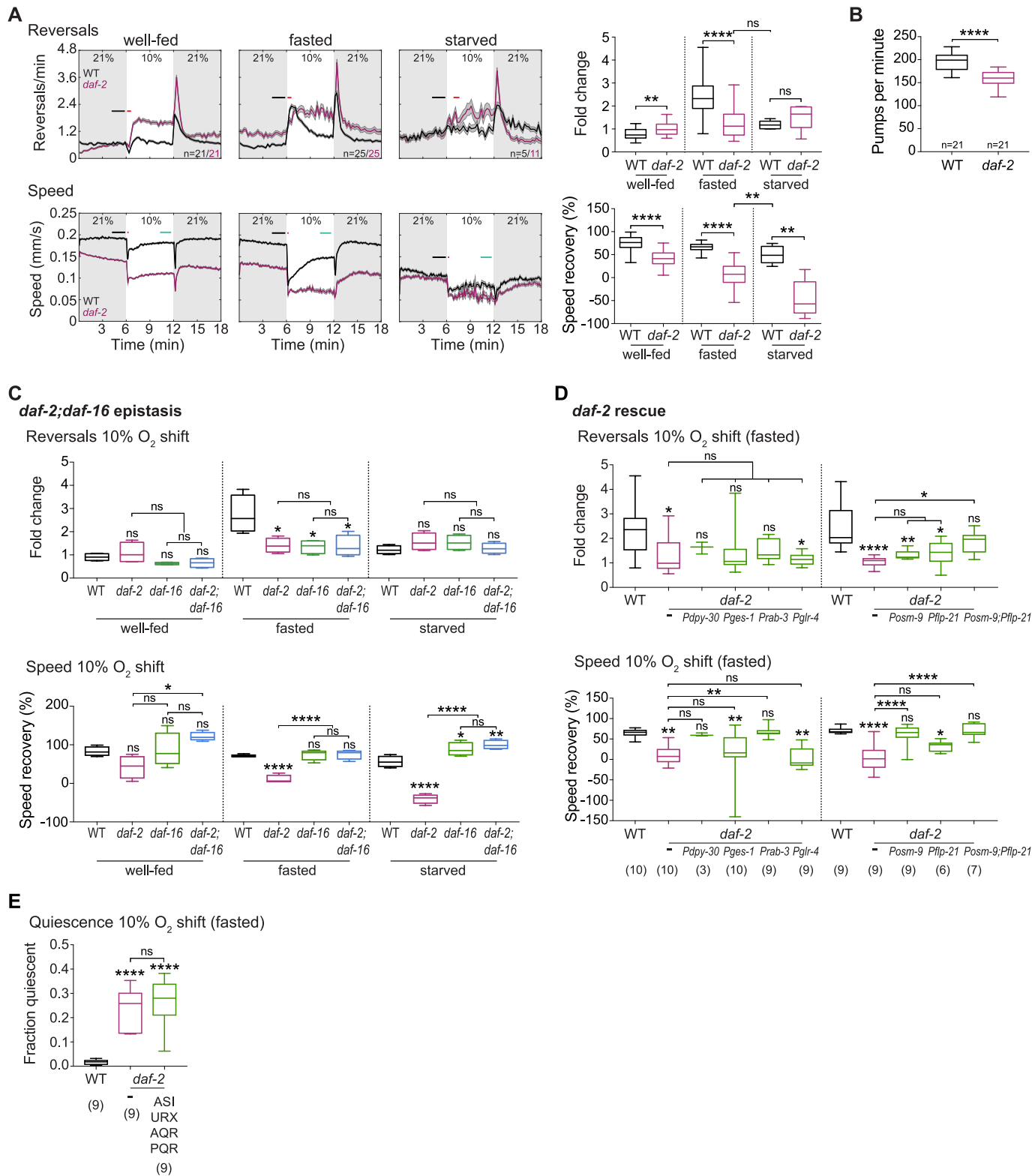


Figure S3. The arousing effect of DAF-2 signaling is dependent on the FOXO transcription factor DAF-16. Related to Figure 2.

(A) Left: Population means (\pm SEM) of indicated behaviors with O₂ stimulation under indicated feeding states. n = number of experiments (40-120 animals each). Right: Quantifications using unpaired t-test (**** p < 0.0001, ** p < 0.01, ns p > 0.05). N-numbers as indicated on the left, except *daf-2* starved, where only experiments performed in parallel to WT were used for quantification (i.e. n = 5 for both WT and *daf-2* starved).

(B) Pharyngeal pumping rates of WT and *daf-2* animals in the presence of food. Number of worms (n) indicated. Unpaired t-test (**** p < 0.0001).

(C) Quantification of *daf-2; daf-16* epistasis experiment for O₂ downshift-dependent behaviors under indicated feeding states, using one-way ANOVA with Sidak's (reversals) or Tukey's (speed) correction (**** p < 0.0001, ** p = 0.0063, * p < 0.05, ns p > 0.05). Significance against WT is indicated above each boxplot. Additional comparisons as shown. Intervals quantified as shown in Figures 1A and 1B. Number of experiments (n) = 4 for each.

(D) Quantification of tissue- and cell-specific *daf-2* rescue experiments in fasted animals. *Pdpy-30*: ubiquitous, *Pges-1*: intestine, *Prab-3*: pan-neuronal, *Pglr-4*: inter- and motor neurons, *Posm-9*: sensory neurons, *Pflp-21*: RMG, FLP, ASJ, M2, URA, URX, ASI. Significance against WT is indicated above each boxplot. Additional comparisons as shown. One-way ANOVA with Sidak's correction (**** p < 0.0001, ** p ≤ 0.01, * p ≤ 0.05, ns p > 0.05). Number of experiments (n) indicated below each boxplot (~40 animals each).

(E) Quantification of rescue experiments in fasted animals driving *daf-2a* cDNA in ASI (using *Pgpa-4*) and URX, AQR, PQR (using *Pgcy-36*) neurons. Quantification interval as shown in Figure 1C. Significance against WT is indicated above each boxplot. One-way ANOVA with Sidak's correction (**** p < 0.0001, ns = 0.6338). Number of experiments (n) indicated below each boxplot (~40 animals each).

For all quantifications, boxplots show median, interquartile range and min to max whiskers.

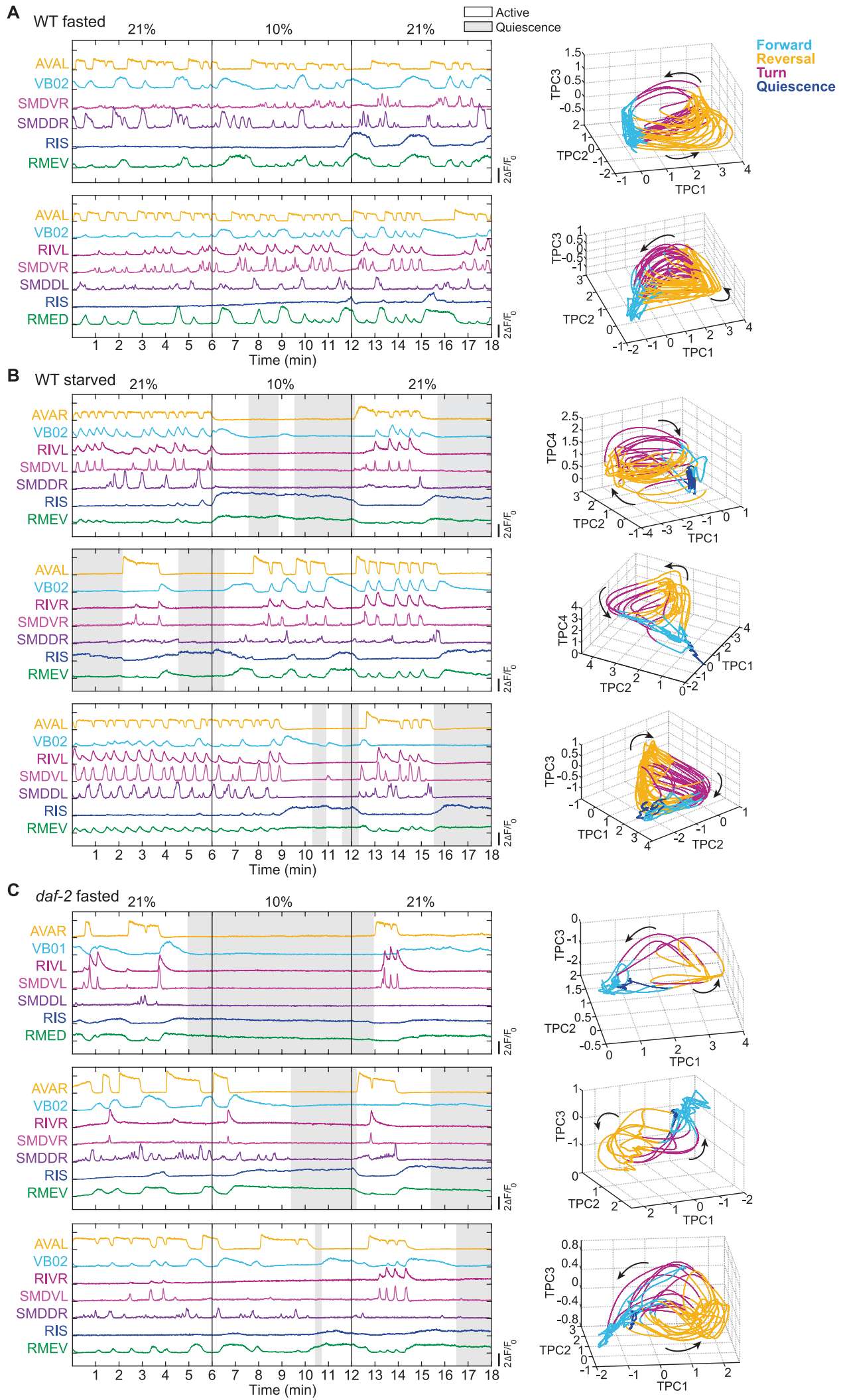


Figure S4. Starvation biases to intermittent neural sleep episodes while insulin signaling maintains continuous neural population dynamics during fasting. Related to Figures 3, 5 and 6.

Additional examples of brain-wide imaging recordings in WT fasted (**A**), WT starved (**B**) and *daf-2* fasted (**C**) worms. Left: Traces show the activity of the reversal interneuron AVA, the forward motor neuron VB02/VB01, the turning motor neurons RIV, SMDV and SMDD, as well as the GABAergic neurons RIS and RMEV/D. O₂ concentration indicated. Grey shadings denote quiescence periods. Right: Phase plot of first 3 integrated principal components (TPCs). Note that for 2 WT starved datasets TPCs 1, 2 and 4 are shown (also see methods). Coloring indicates the respective motor command state and arrows indicate the direction of the trajectory.

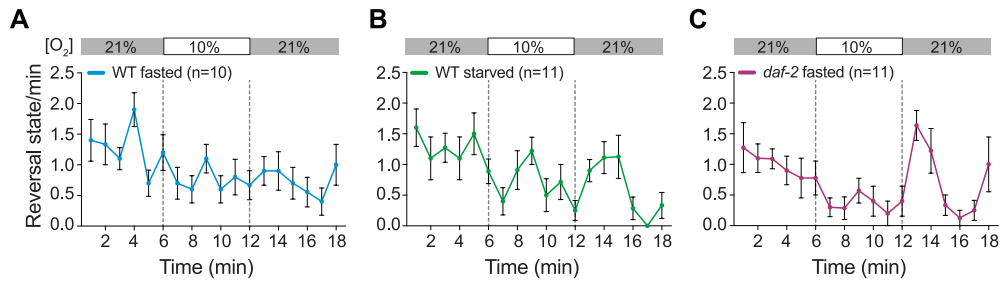


Figure S5. Behavioral regulation downstream of sensory processing is inefficient under imaging conditions in WT but not *daf-2* animals. Related to Figures 3 and 6.

Reversal command state in WT fasted (A), WT starved (B) and *daf-2* fasted (C) brain-wide imaging recordings as read-out by the state of the reversal command interneuron AVA, quantified as mean (\pm SEM) AVA rise phases per minute. Number of recordings (n) indicated.

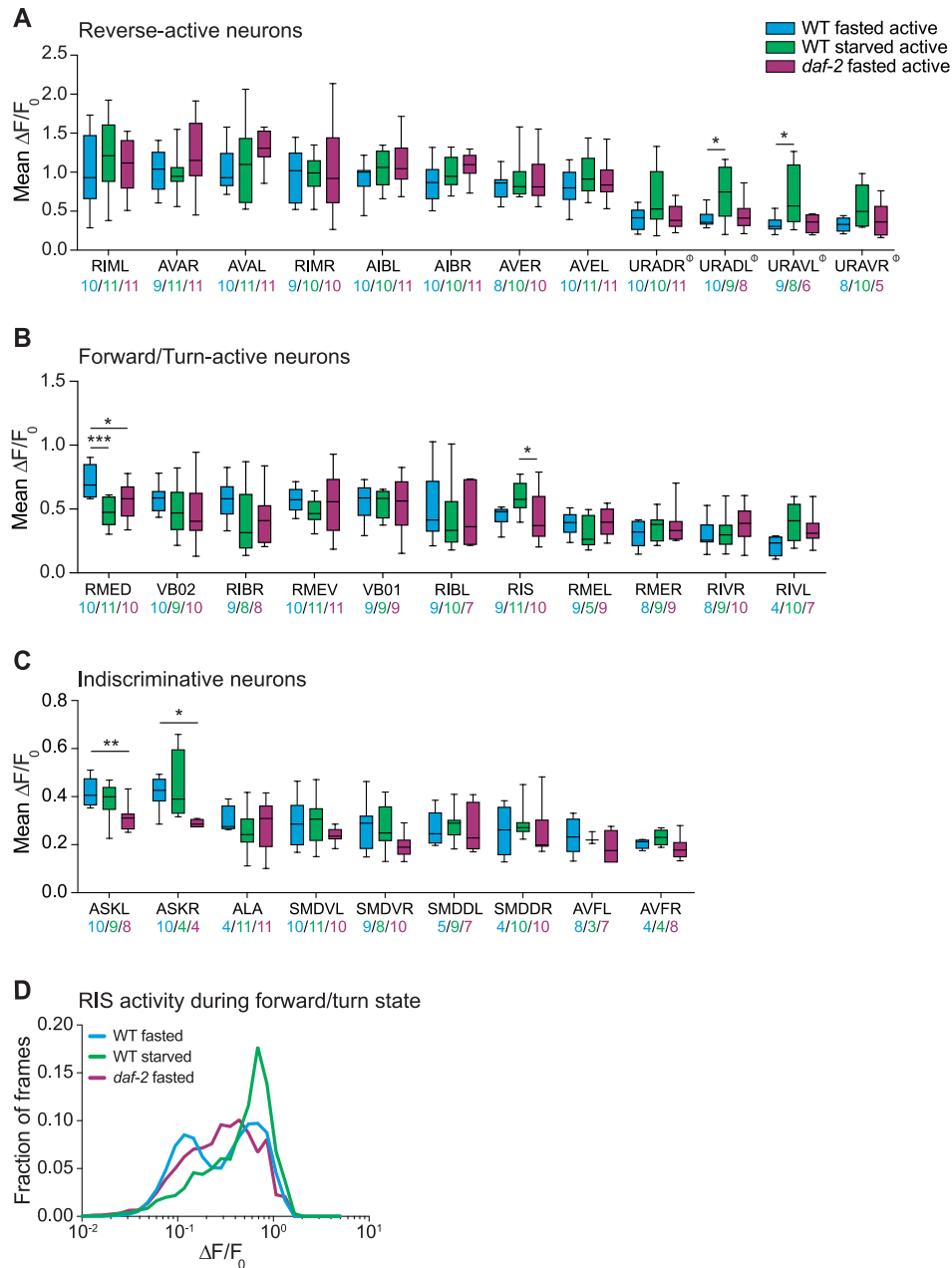


Figure S6. Starvation and mutation in *daf-2* affect the activities of a few neurons during active brain states. Related to Figures 4 and 6.

(A-C) Activity of neurons identified in ≥ 3 recordings. Activity for each neuron was measured during its principal motor command state: reverse-active neurons (A), forward/turn-active neurons (B) or active indiscriminative of motor command state (C) in WT fasted, WT starved and *daf-2* fasted worms, respectively. Boxplots show median, interquartile range and min to max whiskers of mean $\Delta F/F_0$ during the principal active state. Labels indicate putative neuron IDs. Ambiguous IDs are denoted with Φ (see methods for alternatives). Number of data points for each neuron (n) indicated. For each neuron, all conditions were compared against each other using one-way ANOVA with Tukey's correction (***) $p = 0.0002$, ** $p = 0.0046$, * $p \leq 0.05$). Significance levels are only indicated for significant comparisons.

(D) Fractional histograms (log scale) of all RIS $\Delta F/F_0$ values during the forward/turn brain state in WT fasted, WT starved and *daf-2* fasted animals. Number of experiments in which RIS could be identified: WT fasted $n = 9$, WT starved $n = 11$, *daf-2* fasted $n = 10$. Significant differences between the distributions were evaluated using a resampling test, see methods. The resulting p-values were corrected for multiple comparisons using the Bonferroni method and provide an estimate of the probabilities that the measured data in each condition have the same underlying distribution: $p = 3.9 \times 10^{-5}$ (WT fasted versus WT starved), $p = 0.0801$ (WT fasted versus *daf-2* fasted), $p = 6.3 \times 10^{-5}$ (WT starved versus *daf-2* fasted).

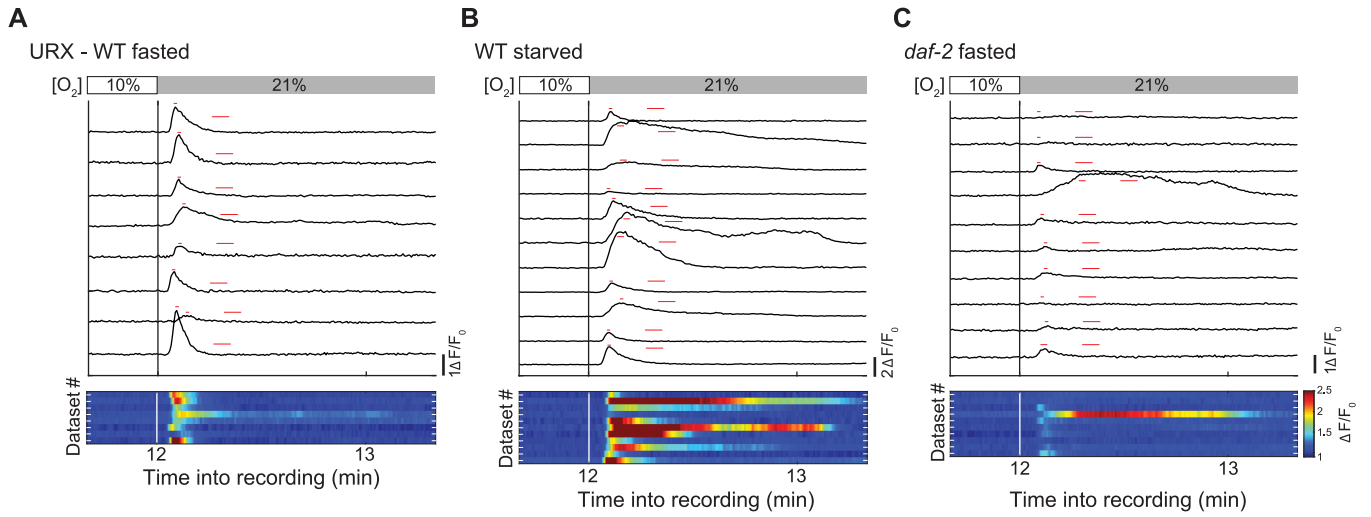


Figure S7. Starvation and *daf-2* modulate URX neuronal activity. Related to Figure 7.

Top: Activities of detected URX neurons per recording for WT fasted (A), WT starved (B) and *daf-2* fasted (C) worms. Shown is the activity of a single URX neuron or, in case both neurons of the bilateral pair were detected, the mean of their activity. Red bars indicate intervals used for quantification in Figure 7D. Bottom: Heat map of URX neuronal activity corresponding to plots on top. O_2 stimulation as indicated.

Table S1. Candidate genetic screen in fasted animals reveals genes involved in O₂ downshift-induced quiescence. Related to Figure 2.

Quantified is fraction quiescent upon fasting during the time interval shown in Figures 1C and 2A for strains with number of experiments (n) ≥ 3. Genes are grouped in categories (indicated in bold) according to biological function and sorted alphabetically within each category.

Significance is determined using one-way ANOVA with Dunnett's correction. Strains significantly different from N2 are emphasized in red.

Gene (allele)	Mean fraction quiescent (± SEM)	Adjusted p-value
N2	0.0113 (± 0.003)	
Neuron differentiation		
<i>ceh-10(ct78)</i>	0.0004 (± 0.0004)	0.9996
<i>ceh-23(ms23)</i>	0.007 (± 0.0044)	0.9998
<i>ceh-36(ks86)</i>	0.0043 (± 0.0037)	0.9997
<i>ceh-37(ok272)</i>	0.003 (± 0.0019)	0.9997
<i>che-1(p679)</i>	0.0018 (± 0.0009)	0.9996
<i>daf-10(e1387)</i>	0.1604 (± 0.0133)	< 0.0001
<i>lin-32(u282)</i>	0.016 (± 0.008)	0.9998
<i>mec-3(e1338)</i>	0.0059 (± 0.0053)	0.9998
<i>odr-3(n2150)</i>	0.0159 (± 0.0103)	0.9998
<i>odr-7(ky4)</i>	0.0035 (± 0.0022)	0.9996
<i>ttx-1(p767)</i>	0.0483 (± 0.0268)	0.9979
<i>ttx-3(mg158)</i>	0.0011 (± 0.0006)	0.9996
<i>unc-130(oy10)</i>	0.00087 (± 0.00087)	0.9996
Growth factor signaling		
<i>age-1(hx546)</i>	0.0196 (± 0.019)	0.9996
<i>akt-1(mg144)</i>	0.0063 (± 0.0029)	0.9997
<i>bra-1(nk1)</i>	0.0043 (± 0.0024)	0.9997
<i>daf-1(m40)</i>	0.0388 (± 0.0187)	0.9986
<i>daf-2(e1370)</i>	0.3058 (± 0.0212)	< 0.0001
<i>daf-3(e1376)</i>	0 (± 0)	0.9996
<i>daf-4(m63)</i>	0.0246 (± 0.0156)	0.9994
<i>daf-16(mu86)</i>	0.0105 (± 0.0036)	0.9999
<i>dbl-1(wk70)</i>	0.0009 (± 0.0005)	0.9996
<i>ins-1(nr2091)</i>	0.0125 (± 0.0049)	0.9999
<i>ins-7(tm1907)</i>	0.0037 (± 0.0037)	0.9997
<i>ins-10(tm3498)</i>	0.0094 (± 0.0047)	0.9999
<i>ist-1(ok2706)</i>	0.0204 (± 0.0063)	0.9996
<i>sma-6(e1482)</i>	0.016 (± 0.0055)	0.9998
G protein signaling		
<i>ags-3(ok1169)</i>	0.1276 (± 0.0497)	0.0052
<i>egl-30(ad806)</i>	0.0021 (± 0.0021)	0.9996
<i>egl-30(js126)</i>	0.0078 (± 0.0055)	0.9999
<i>gar-3(vu78)</i>	0.0754 (± 0.0388)	0.5542
<i>goa-1(sa734)</i>	0.0221 (± 0.0082)	0.9996
<i>gpa-6(pk480)</i>	0.0088 (± 0.0044)	0.9999
<i>gpa-8(pk345)</i>	0.0246 (± 0.005)	0.9994
<i>gpa-10(pk362)</i>	0.0091 (± 0.0044)	0.9999
<i>gpb-2(ad451)</i>	0.0745 (± 0.0493)	0.5791
<i>grk-2(gk268)</i>	0.1204 (± 0.0276)	0.0123

<i>grk-2(rt97)</i>	0.2013 (\pm 0.0546)	< 0.0001
<i>gsa-1(ce81)</i>	0.0011 (\pm 0.0005)	0.9996
<i>odr-4(n2144)</i>	0.0075 (\pm 0.0075)	0.9999
<i>rgs-2(vs17)</i>	0.0077 (\pm 0.0025)	0.9998
Metabolism		
<i>aak-2(gt33)</i>	0.0017 (\pm 0.001)	0.9992
<i>aak-2(rr48)</i>	0.011 (\pm 0.0054)	0.9999
<i>fat-3(wa22)</i>	0.0092 (0.0024)	0.9999
<i>nhr-49(ok2165)</i>	0.0698 (\pm 0.0176)	0.7177
<i>ogt-1(ok430)</i>	0.0098 (\pm 0.0056)	0.9999
<i>pept-1(lg1601)</i>	0.0088 (\pm 0.0015)	0.9999
Neurotransmitter		
<i>bas-1(tm351)</i>	0.0058 (\pm 0.0017)	0.9997
<i>cat-1(e1111)</i>	0.0274 (\pm 0.0095)	0.9993
<i>cat-2(e1112)</i>	0.0321 (\pm 0.0203)	0.9996
<i>cat-4(e1141)</i>	0.0158 (\pm 0.0104)	0.9998
<i>dat-1(ok157)</i>	0.0046 (\pm 0.0014)	0.9997
<i>dop-5(ok568)</i>	0.0059 (\pm 0.0006)	0.9998
<i>dop-6(ok2090)</i>	0.0032 (\pm 0.0028)	0.9997
<i>eat-2(ad465)</i>	0.0076 (\pm 0.0034)	0.9999
<i>eat-4(ky5)</i>	0.0032 (\pm 0.0019)	0.9995
<i>egl-3(n150)</i>	0.0185 (\pm 0.0177)	0.9997
<i>flp-34(ok3071)</i>	0.005 (\pm 0.0003)	0.9997
<i>glt-1(ok206)</i>	0.0048 (\pm 0.0026)	0.9997
<i>glt-3(bz34)</i>	0.0113 (\pm 0.0055)	0.9999
<i>glt-5(ok1987)</i>	0.0113 (\pm 0.0054)	0.9999
<i>glt-6(tm1316)</i>	0.0201 (\pm 0.0096)	0.9996
<i>glt-7(tm1641)</i>	0.0156 (\pm 0.0046)	0.9998
<i>nlp-15(ok1512)</i>	0.0049 (\pm 0.0021)	0.9997
<i>nmur-1(ok1387)</i>	0.0028 (\pm 0.0018)	0.9997
<i>nmur-2(ok3502)</i>	0.0008 (\pm 0.0008)	0.9996
<i>npr-9(tm1652)</i>	0.0068 (\pm 0.0061)	0.9998
<i>ntc-1(tm2385)</i>	0.0173 (\pm 0.0086)	0.9997
<i>ntr-1(tm2765)</i>	0.0093 (\pm 0.0059)	0.9999
<i>ntr-2(tm2243)</i>	0.0158 (\pm 0.0088)	0.9998
<i>sbt-1(ok901)</i>	0.0047 (\pm 0.0028)	0.9997
<i>ser-2(ok2103)</i>	0.0086 (\pm 0.0029)	0.9999
<i>tph-1(mg280)</i>	0.0065 (\pm 0.0045)	0.9999
<i>unc-31(e928)</i>	0.0091 (\pm 0.0053)	0.9996
Various		
<i>crh-1(tz2)</i>	0.0133 (\pm 0.0046)	0.9999
<i>daf-22(m130)</i>	0.0049 (\pm 0.0042)	0.9997
<i>egl-4(ad450)</i>	0.0009 (\pm 0.0005)	0.9996
<i>egl-4(n478)</i>	0.0146 (\pm 0.0119)	0.9996
<i>egl-9(sa307)</i>	0.0559 (\pm 0.0227)	0.9789
<i>inx-1(tm3524)</i>	0.0105 (\pm 0.0068)	0.9999
<i>inx-4(tm3276)</i>	0.0024 (\pm 0.0024)	0.9996
<i>inx-14(ag17)</i>	0.0113 (\pm 0.0046)	0.9999
<i>inx-19(ky634)</i>	0.0659 (\pm 0.0058)	0.8239
<i>itr-1(sa73)</i>	0.0274 (\pm 0.0065)	0.9993
<i>jdk-1(km2)</i>	0.0784 (\pm 0.0375)	0.4727
<i>ocr-2(ak47)</i>	0.0026 (\pm 0.0001)	0.9996
<i>trp-4(gk341)</i>	0.0133 (\pm 0.0042)	0.9999

<i>trp-4(ok1605)</i>	0.0103 (\pm 0.0061)	0.9999
<i>unc-43(n498n1186)</i>	0.0062 (\pm 0.0052)	0.9998
<i>unc-68(e540)</i>	0.0096 (\pm 0.0049)	0.9999

Supplemental experimental procedures

Worm strains and maintenance

Worms were maintained under standard laboratory conditions on nematode growth medium (NGM) plates seeded with *Escherichia coli* OP50 as bacterial food source. Strains were kept at 20°C, except for strains carrying a temperature-sensitive conditional mutation (see below). The wild type strain used was *C. elegans* Bristol N2. All strains are listed in the table below.

Strain list. Strains are listed in order of appearance, followed by a list of strains exclusively used for candidate genetic screen (Table S1).

Strain	Information	Genotype (and injection concentration, if applicable)	Source
N2	wild type		Caenorhabditis Genetics Center
CX11697	genetic BAG and ASG ablation	<i>kyIs536[Pflp-17::p17::SL2::gfp; elt-2::mCherry]; kyIs538[Pglb-5::p12::SL2::gfp; elt-2::mCherry]</i>	Cori Bargmann, Rockefeller University
CX7102	genetic URX, AQR, PQR ablation	<i>lin-15(n765); qals2241[gcy-36::egl-1; gcy-35::gfp; lin-15(+)] X</i>	Cori Bargmann, Rockefeller University
CX11735	genetic BAG, ASG, URX, AQR, PQR ablation	<i>kyIs536[Pflp-17::p17::SL2::gfp; elt-2::mCherry]; kyIs538[Pglb-5::p12::SL2::gfp; elt-2::mCherry]; lin-15(n765); qals2241[gcy-36::egl-1; gcy-35::gfp; lin-15(+)] X</i>	Cori Bargmann, Rockefeller University
ZIM426	genetic RMG ablation	<i>mzmEx252[Pglr-4::p12::SL2::mCherry (25ng/μl); Punc-122::dsRed (15ng/μl)]; mzmEx251[Pncs-1::p17::SL2::mCherry (5ng/μl); Punc-122::gfp (15ng/μl)]</i>	This study
JY190		<i>osm-9(yz6) IV</i>	Caenorhabditis Genetics Center
CX6448		<i>gcy-35(ok769) I</i>	Cori Bargmann, Rockefeller University
AX2197		<i>gcy-36(db66) X</i>	Cori Bargmann, Rockefeller University
CB1370		<i>daf-2(e1370) III</i>	Caenorhabditis Genetics Center
CF1038		<i>daf-16(mu86) I</i>	Caenorhabditis Genetics Center
ZIM919		<i>daf-16(mu86) I; daf-2(e1370) III</i>	This study
JN1515	ubiquitous <i>daf-2</i> rescue	<i>daf-2(e1370) III; Ex[Pdpy-30::daf-2a; Pmyo-3::venus]</i>	Yuichi Iino, University of Tokyo, Ohno et al., 2014
ZIM1025	pan-neuronal <i>daf-2</i> rescue	<i>daf-2(e1370) III; mzmEx628[Prab-3::daf-2a::SL2::mCherry (10ng/μl); Punc-122::dsRed (15ng/μl)]</i>	This study
ZIM1016	intestinal <i>daf-2</i> rescue	<i>daf-2(e1370) III; mzmEx620[Pges-1::daf-2a::SL2::mCherry (30ng/μl); Punc-122::dsRed (15ng/μl)]</i>	This study
ZIM1341	inter-/motor neuron <i>daf-2</i> rescue	<i>daf-2(e1370) III; mzmEx813[Pglr-4::daf-2a::SL2::mCherry (25ng/μl); Punc-122::dsRed (15ng/μl)]</i>	This study

ZIM1303	sensory neuron <i>daf-2</i> rescue	<i>daf-2(e1370) III; mzmEx790[Pposm-9::daf-2a::SL2::mCherry::osm-9-3'UTR (30ng/μl); Punc-122::dsRed (15ng/μl)]</i>	This study
ZIM1394	<i>Pflp-21 daf-2</i> rescue	<i>daf-2(e1370) III; mzmEx845[Pflp-21::daf-2a::SL2::mCherry (20ng/μl); Punc-122::dsRed (15ng/μl)]</i>	This study
ZIM1580	<i>Pflp-21</i> reporter line	<i>daf-2(e1370) III; mzmEx943[Pflp-21::mCherry (20ng/μl); Punc-122::gfp (15ng/μl)]</i>	This study
ZIM1326	<i>Pflp-21</i> plus sensory neuron <i>daf-2</i> rescue	<i>daf-2(e1370) III; mzmEx801[Pflp-21::daf-2a::SL2::mCherry (20ng/μl); Posm-9::daf-2a::SL2::mCherry::osm-9-3'UTR (30ng/μl); Punc-122::dsRed (15ng/μl)]</i>	This study
ZIM1393	<i>Pglr-4; Posm-9</i> expression pattern overlap	<i>daf-2(e1370) III; mzmEx4[Pglr-4::gfp (30ng/μl); Punc-122::dsRed (15ng/μl)]; mzmEx790[Pposm-9::daf-2a::SL2::mCherry::osm-9-3'UTR (30ng/μl); Punc-122::dsRed (15ng/μl)]</i>	This study
ZIM1206	ASI + URX, AQR, PQR <i>daf-2</i> rescue	<i>daf-2(e1370) III; mzmEx732[Pgpa-4::daf-2a::SL2::mCherry (40ng/μl); Pgcy-36::daf-2a::SL2::mCherry (1.5ng/μl); Punc-122::dsRed (15ng/μl)]</i>	This study
ZIM1048	WT whole-brain imaging line	<i>lite-1(ce314) X; mzmIs4[Punc-31::NLS-GCaMP5K; Punc-122::gfp]</i>	Kato et al., 2015
ZIM1107	<i>daf-2</i> whole-brain imaging line	<i>daf-2(e1370) III; lite-1(ce314) X; mzmIs4[Punc-31::NLS-GCaMP5K; Punc-122::gfp]</i>	This study
ZIM1181	ASK marker whole-brain imaging line	<i>lite-1(ce314) X; mzmIs4[Punc-31::NLS-GCaMP5K; Punc-122::gfp]; mzmEx706[Psrbc-64::NLSwCherryNLS (25ng/μl); Punc-122::dsRed (15ng/μl)]</i>	This study
Strains exclusively used for candidate genetic screen (Table S1)			
Strain	Genotype	Additional information	Source
ZIM177	<i>aak-2(gt33) X</i>	6x outcrossed from strain TG33 (Caenorhabditis Genetics Center)	This study
MR507	<i>aak-2(rr48) X</i>		Caenorhabditis Genetics Center
TJ1052	<i>age-1(hx546) I</i>		Caenorhabditis Genetics Center
RB1145	<i>ags-3(ok1169) X</i>		Caenorhabditis Genetics Center
GR1310	<i>akt-1(mgl44) V</i>		Caenorhabditis Genetics Center
LC33	<i>bas-1(tm351) III</i>		Caenorhabditis Genetics Center
NU1	<i>bra-1(nk1) X</i>		Caenorhabditis Genetics Center
CB1111	<i>cat-1(e1111) X</i>		Caenorhabditis Genetics Center
CB1112	<i>cat-2(e1112) II</i>		Caenorhabditis Genetics Center
CB1141	<i>cat-4(e1141) V</i>		Caenorhabditis Genetics Center
BW506	<i>ceh-10(ct78) III</i>		Caenorhabditis Genetics Center
OH149	<i>ceh-23(ms23) III</i>		Caenorhabditis Genetics Center

FK311	<i>ceh-36(ks86) X</i>		Caenorhabditis Genetics Center
LJ1	<i>ceh-37(ok272) X</i>		Caenorhabditis Genetics Center
PR679	<i>che-1(p679) I</i>		Caenorhabditis Genetics Center
YT17	<i>crh-1(tz2) III</i>		Caenorhabditis Genetics Center
DR40	<i>daf-1(m40) IV</i>		Caenorhabditis Genetics Center
CB1376	<i>daf-3(e1376) X</i>		Caenorhabditis Genetics Center
DR63	<i>daf-4(m63) III</i>		Caenorhabditis Genetics Center
CB1387	<i>daf-10(e1387) IV</i>		Caenorhabditis Genetics Center
DR476	<i>daf-22(m130) II</i>		Caenorhabditis Genetics Center
RM2702	<i>dat-1(ok157) III</i>		Caenorhabditis Genetics Center
LT121	<i>dbl-1(wk70) V</i>		Caenorhabditis Genetics Center
RB785	<i>dop-5(ok568) V</i>		Caenorhabditis Genetics Center
RB1680	<i>dop-6(ok2090) X</i>		Caenorhabditis Genetics Center
DA465	<i>eat-2(ad465) II</i>		Caenorhabditis Genetics Center
CX13503	<i>eat-4(ky5) III</i>		Cori Bargmann, Rockefeller University
CX9191	<i>egl-3(n150) V</i>		Cori Bargmann, Rockefeller University
DA521	<i>egl-4(ad450) IV</i>		Caenorhabditis Genetics Center
MT1073	<i>egl-4(n478) IV</i>		Caenorhabditis Genetics Center
JT307	<i>egl-9(sa307) V</i>		Caenorhabditis Genetics Center
DA1084	<i>egl-30(ad806) I</i>		Caenorhabditis Genetics Center
NM1380	<i>egl-30(js126) I</i>		Caenorhabditis Genetics Center
BX30	<i>fat-3(wa22) IV</i>		Caenorhabditis Genetics Center
RB2269	<i>flp-34(ok3071) V</i>		Caenorhabditis Genetics Center
JD217	<i>gar-3(vu78) V</i>		Caenorhabditis Genetics Center
ZIM637	<i>glt-1(ok206) X</i>	isolated from strain ZB1106 (Caenorhabditis Genetics Center)	This study
ZIM648	<i>glt-3(bz34) IV</i>		Itzhak Mano, City University of New

			York, Mano et al., 2007
RB1615	<i>glt-5(ok1987) II</i>		Caenorhabditis Genetics Center
ZIM728	<i>glt-6(tm1316) IV</i>	5x outcrossed from strain FX01316 (National Bioresource Project)	This study
ZIM711	<i>glt-7(tm1641) IV</i>	4x outcrossed from strain FX01641 (National Bioresource Project)	This study
DG1856	<i>goa-1(sa734) I</i>		Caenorhabditis Genetics Center
NL1146	<i>gpa-6(pk480) X</i>		Caenorhabditis Genetics Center
NL1142	<i>gpa-8(pk345) V</i>		Caenorhabditis Genetics Center
NL1147	<i>gpa-10(pk362) V</i>		Caenorhabditis Genetics Center
DA541	<i>gpb-2(ad541) I</i>		Caenorhabditis Genetics Center
FG7	<i>grk-2(gk268) III</i>		Caenorhabditis Genetics Center
HA865	<i>grk-2(rt97) III</i>		Caenorhabditis Genetics Center
KG421	<i>gsa-1(ce81) I</i>		Caenorhabditis Genetics Center
CX7155	<i>ins-1(nr2091) IV</i>		Cori Bargmann, Rockefeller University
FX01907	<i>ins-7(tm1907) IV</i>		National Bioresource Project
FX03498	<i>ins-10(tm3498) V</i>		National Bioresource Project
CX12016	<i>inx-1(tm3524) X</i>		Cori Bargmann, Rockefeller University
FX03276	<i>inx-4(tm3276) V</i>		National Bioresource Project
AU98	<i>inx-14(ag17) I</i>		Caenorhabditis Genetics Center
CX6161	<i>inx-19(ky634) I</i>		Caenorhabditis Genetics Center
RB2621	<i>ist-1(ok2706) X</i>		Caenorhabditis Genetics Center
JT73	<i>itr-1(sa73) IV</i>		Caenorhabditis Genetics Center
KU2	<i>jkk-1(km2) X</i>		Caenorhabditis Genetics Center
TU282	<i>lin-32(u282) X</i>		Caenorhabditis Genetics Center
CB1338	<i>mec-3(e1338) IV</i>		Caenorhabditis Genetics Center
RB1716	<i>nhr-49(ok2165) I</i>		Caenorhabditis Genetics Center
VC1063	<i>nlp-15(ok1512) I</i>		Caenorhabditis Genetics Center

RB1288	<i>nmur-1(ok1387) X</i>		Caenorhabditis Genetics Center
RB2526	<i>nmur-2(ok3502) II</i>		Caenorhabditis Genetics Center
IC683	<i>npr-9(tm1652) X</i>		Caenorhabditis Genetics Center
FX02385	<i>ntc-1(tm2385) X</i>		National Bioresource Project
FX02765	<i>ntr-1(tm2765) I</i>		National Bioresource Project
FX02243	<i>ntr-2(tm2243) I</i>		National Bioresource Project
CX4544	<i>ocr-2(ak47) IV</i>		Caenorhabditis Genetics Center
CX2205	<i>odr-3(n2150) V</i>		Caenorhabditis Genetics Center
MT5300	<i>odr-4(n2144) III</i>		Caenorhabditis Genetics Center
CX4	<i>odr-7(ky4) X</i>		Caenorhabditis Genetics Center
RB653	<i>ogt-1(ok430) III</i>		Caenorhabditis Genetics Center
BR2742	<i>pept-1(lg1601) X</i>		Caenorhabditis Genetics Center
LX160	<i>rgs-2(vs17) X</i>		Caenorhabditis Genetics Center
RB987	<i>sbt-1(ok901) V</i>		Caenorhabditis Genetics Center
RB1690	<i>ser-2(ok2103) X</i>		Caenorhabditis Genetics Center
CB1482	<i>sma-6(e1482) II</i>		Caenorhabditis Genetics Center
MT15434	<i>tph-1(mg280) II</i>		Caenorhabditis Genetics Center
VC818	<i>trp-4(gk341) I</i>		Caenorhabditis Genetics Center
VC1141	<i>trp-4(ok1605) I</i>		Caenorhabditis Genetics Center
PR767	<i>ttx-1(p767) V</i>		Caenorhabditis Genetics Center
OH8	<i>ttx-3(mg158) X</i>		Caenorhabditis Genetics Center
DA509	<i>unc-31(e928) IV</i>		Caenorhabditis Genetics Center
MT2605	<i>unc-43 (n498n1186) IV</i>		Caenorhabditis Genetics Center
CB540	<i>unc-68(e540) V</i>		Caenorhabditis Genetics Center
PY1133	<i>unc-130(oy10) II</i>		Caenorhabditis Genetics Center

Note on genetic RMG ablation strain (ZIM426):

The two promoters used for split caspase expression (Chelur and Chalfie, 2007) in RMG also overlapped in additional neurons posterior to the nerve ring, likely SMDV or SAAV; occasional overlap in an additional neuron class was observed, likely AVH or AVJ. Therefore, these neurons might be ablated as well.

Molecular biology and transgenesis

Promoters were PCR-amplified from either whole-worm genomic DNA or indicated plasmid (see table below) and, flanked by restriction sites, cloned into pSM vector. Promoters were inserted using *FseI* and *AscI* restriction sites. For the *Posm-9* construct, the *unc-54* 3'UTR of pSM vector was replaced with *osm-9* 3'UTR.

A plasmid containing *daf-2a* cDNA was kindly provided by the Iino laboratory (Ohno et al., 2014). *daf-2a* cDNA was amplified from this plasmid and inserted into pSM vector using *NheI* and *KpnI* restriction sites.

Transgenic lines were generated using standard microinjection techniques. In brief, plasmids were injected into the gonads of young adult hermaphrodites, thereby generating heritable extrachromosomal arrays. All injection mixes contained a total of 100 ng/μl DNA. All plasmids are listed in the table below.

Oligonucleotides used for amplification of tissue- and cell-specific promoter fragments. Fwd indicates forward primer, Rev indicates reverse primer sequence. Number in brackets shows the length of the generated fragment.

Gene	Sequence (5' → 3')	Notes
<i>ges-1</i>	Fwd: GCATAGCCCCGAGTCAC Rev: CTGAATTCAAAGATAAGATATGTAATA (1931 bp)	amplified from plasmid pJH668, a kind gift from the Zhen lab
<i>rab-3</i>	Fwd: GATCTTCAGATGGGAGCA Rev: CTGAAAATAGGGCTACTG (1208 bp)	
<i>glr-4</i>	Fwd: GGAGCACAAACGAGAAGACC Rev: GCTGTGTAAAAGTTTAGCTCATC (4392 bp)	
<i>osm-9</i>	Promoter Fwd: ACGTACGATTATCTGTTGCG Promoter Rev: CCAATTTTTTCAGAAACCAAAC (1744 bp) 3'UTR Fwd: GAACTTTTTTCTTCTA 3'UTR Rev: TCGTCTCTATTCTAAATTGC (3520 bp)	
<i>flp-21</i>	Fwd: TGAGGTCACGCAACTTGATGATC Rev: GAAAATGACTTTTTGGATTTTGG (4099 bp)	amplified from plasmid pEM1, a kind gift from the Bargmann lab
<i>gcy-36</i>	Fwd: ATGATGTTGGTAGATGGGGTTTGG Rev: AAATTCAAACAAGGGCTACCCAACA (1087 bp)	
<i>gpa-4</i>	Fwd: CGATGATCATTGGAAATGCGGTTTCC Rev: TGTTGAAAAGTGTTACAAAATGAATAAGTGG (2783 bp)	

Expression patterns of promoters used for transgenic rescues

Pdpy-30: ubiquitous (Ohno et al., 2014)

Pges-1: intestine (Hung et al., 2014)

Prab-3: pan nervous system (Nonet et al., 1997)

Pglr-4: AVA, RMD, SMD, SAA, SIB, RIB, RIM, AVH, FLP, RMG, DVA, AUA, PVD, URY, URA, SAB, RIF, DB, PVU (Brockie et al., 2001)

Posm-9: OLQ, IL2, AWA, AWC, ASE, ADF, ASG, ASH, ASI, ASJ, ASK, ADL, FLP, PVD, PHA, PHB (Colbert et al., 1997)

Pflp-21: RMG (100%), ASJ (100%), URA (100%), FLP (100%), M2 (100%), URX (80%), ASI (10%), 2-3 tail neurons (100%) (assessed using a *daf-2(e1370)*; *Pflp-21::mCherry* reporter line)

Pgpa-4: ASI (Jansen et al., 1999)

Pgcy-36: URX, AQR, PQR (Gray et al., 2004)

Plasmid list.

Plasmids used in this study (plasmid no)	Source
Pglr-4::p12::SL2::mCherry (pRL87)	This study
Pncs-1::p17::SL2::mCherry (pRL58)	This study
Prab-3::daf-2a::SL2::mCherry (pSS92)	This study
Pges-1::daf-2a::SL2::mCherry (pSS91)	This study
Pglr-4::daf-2a::SL2::mCherry (pSS96)	This study
Posm-9::daf-2a::SL2::mCherry::osm-9 3'UTR (pFM5)	This study
Pflp-21::daf-2a::SL2::mCherry (pFM6)	This study
Pglr-4::gfp (pIH4)	This study
Pgpa-4::daf-2a::SL2::mCherry (pFM4)	This study
Pgcy-36::daf-2a::SL2::mCherry (pFM2)	This study
Psrbc-64::NLSwCherryNLS (pTS113)	Kato et al., 2015
Pflp-21::mCherry (pRL49)	This study
Punc-122::dsRed	Cori Bargmann, Rockefeller University
Punc-122::gfp	Cori Bargmann, Rockefeller University

Worm population behavioral recordings

Worm population behavioral recordings were performed at 20°C as described previously (Hums et al., 2016; Zimmer et al., 2009), with some modifications. For each assay, ~100 one-day old adult hermaphrodites were manually transferred onto a bacteria-free 14 cm NGM agar assay plate. For well-fed assays, transfer time was kept consistent and limited to 10 minutes. Well-fed assays were started 12-14 minutes after the start of assay preparation. For fasted assays, the same animals and plates as for well-fed assays were re-examined. For starved assays, animals were transferred to 15 cm glass petri dishes containing NGM agar plus 25 µg/ml carbenicillin to prevent growth of bacterial food sources during starvation period. Animals were transferred from starvation plates to NGM assay plates after 15 hours of starvation and allowed to settle for one additional hour before the assay commenced. Animals were constrained to a recording region (56 x 56 mm) by creating an arena that was delimited by Whatman filter paper soaked in 20 mM of the repellent copper chloride. Gas flow was achieved by placing a custom-made plexiglass device with a flow arena of 60 x 60 x 0.7 mm onto the assay arena. Gas flow was set to 100 ml/min and controlled using a static gas mixer connected to mass flow controllers (Vögtlin Instruments AG) that were operated by custom-written LabVIEW software (National Instruments). The recording area was illuminated with a 200 mm x 200 mm flat red LED. Recordings were acquired at 3 frames per seconds (fps) on a 4-5 megapixel CCD camera (JAI) using StreamPix software (NorPix). Pixel resolution was 0.0276 mm/pixel.

Temperature-sensitive *daf-2(e1370)* mutants, all *daf-2* rescue strains and corresponding N2 controls were maintained at the permissive temperature of 16°C to prevent developmental arrest (Gems et al., 1998). For well-fed and fasted assays, food plates with animals were shifted to 25°C in the evening before the experiment, allowing a minimal time of 16 hours at the restrictive temperature. The food plates were placed in the experiment room (20 ± 1°C) 2 hours before the start of the experiment to avoid artefacts due to sudden temperature shifts. The subsequent preparation of well-fed and fasted assays was performed as described above for non-temperature-sensitive strains. For starved experiments, food plates with animals were shifted to restrictive 25°C approximately 7 hours before starvation commenced. Animals were then transferred onto pre-warmed starvation plates and starved at 25°C. After 14 hours of starvation, starved plates were placed in the experiment room to accommodate animals to the ambient temperature in the room. After 15 hours, starved animals were transferred onto the assay plate and allowed to settle for one additional hour, as described above for non-temperature-sensitive strains. The gas flow rate for temperature-sensitive strains and their controls was adjusted to 50 ml/min to minimize their arena-leaving behavior.

For experiments shown in Figures 1E and 1F, worms were transferred from the starvation plates to the assay plates after 14 hours of starvation, allowed to settle for one additional hour as described above and the recordings were started after 15 hours of starvation.

All gas mixtures were balanced with nitrogen (N₂).

For the data shown in Figure S1B and Movie S1, worm population recordings were performed using the same setup, with some modifications to obtain higher spatial and temporal resolution (pixel resolution: 0.0129 mm/pixel, frame rate: 10 frames per second), as described previously (Hums et al., 2016). The recording region for these experiments

was 36 x 36 mm and gas flow with a flow rate of 25 ml/min was achieved using a plexiglass device with a flow arena of 39 x 39 x 0.7 mm. Single movie frames shown in Figures 1A-1D were taken from experiments performed with these settings.

Video tracking of animal behavior

Tracking and analysis were performed using customized MATLAB scripts that are based on the Parallel Worm Tracker (Hums et al., 2016; Ramot et al., 2008; Zimmer et al., 2009). In brief, each frame was converted into a binary image using an intensity threshold. Worms were identified as objects in a defined size range. The worm's centroid was determined using the MATLAB regionprops function and worm trajectories over time were created by connecting nearby centroid coordinates in adjacent frames. For each identified worm object, centroid coordinates as outlined above, size in pixels, direction in degrees, speed and eccentricity were calculated. Trajectories were terminated when objects collide with each other or with the boundaries of the arena. Trajectories below a length of 20 frames (i.e. 6.67 sec) were discarded. The behavior of each worm is therefore represented by several worm tracks of varying lengths but not overlapping in time.

Worm speed was calculated by smoothing the worm trajectories. The worm speed in each track was normalized to the median size of N2 wild type worms to account for speed variability arising from difference in size. Backward locomotion (= reversals) was detected by characteristic changes in angular velocity. Omega turns (= deep body bends leading to re-orientation) were detected based on the co-occurrence of an increase in angular velocity and a decrease in eccentricity within a specific range. Reversal and omega turn frequencies were calculated in bins of 45 frames (= 15 seconds). Average speed and average reversal frequencies shown are calculated only from worms that were in their active phase (except for Figure S2D), i.e. data points at which a worm was found to be quiescent or head-waving were taken out from the calculation. Speed data only contain forward movement, i.e. in addition to excluding quiescent/head-waving periods, time points at which worms were found reversing or turning were excluded from calculations.

Determination of quiescence and head-waving episodes

We distinguished 2 immobile states: quiescence (Q) and head-waving (H), the latter of which was characterized by retained dorso-ventral movement of the head/neck region. Both states were determined in 1 sec bins. Tracks of less than 60 frames (i.e. 20 sec) as well as tracks in which the mean speed over the entire track was less than 0.006 mm/s were excluded to avoid tracking of dead objects. The state detection relied on threshold values of speed (1 sec binning) and the instantaneous change in object eccentricity ($d\epsilon/dt$) (1 sec binning and subsequently smoothed using a 5 sec running average) to detect head and body movement. Thresholds were as follows and determined empirically: 0.02 (Q) and 0.025 (H) for speed and 0.00107 (Q and H) for $d\epsilon/dt$ (Figure S1C). Quiescence was determined for the center frame of a 10 sec sliding window if animals exceeded the Q thresholds for less than 20% of time in the sliding window. Head-waving was determined by animals exceeding the H speed and $d\epsilon/dt$ thresholds for < 20% and > 80% of time in a 20 sec sliding window, respectively. Quiescence (head-waving) episodes required to be at least 10 (15) sec in length. The minimal length thresholds for quiescence and head-waving have been determined empirically by manual inspection of behavioral recordings of individual worms. During these inspections, we found that there existed lasting and continuous episodes that were characterized by low speed in combination with either the presence or absence of head movement. The thresholds allow to find these states as 'pure' states as opposed to e.g. quiescence periods that are frequently interspersed with short head movements.

It should be noted that the resolution of the experimental setup did not allow unambiguous distinction of quiescence and head-waving states, because eccentricity changes due to head-waving could only be detected if the head moved in x-y direction. Movement in z is unreliably resolved and some head-waving periods might falsely be assigned to quiescence.

All plots and quantifications showing activity and quiescence, respectively, exclude head-waving behavior.

Skeletonization and segment angle time series

This analysis was performed on behavioral data recorded at higher temporal and spatial resolution (see 'Worm population behavioral recordings'). To obtain the segment angle time series depicted in Figure S1B, the binary worm images resulting from the image processing during tracking (see 'Video tracking of animal behavior') were skeletonized as described previously (Hums et al., 2016), resulting in 25 equally spaced body segments. The angles shown in Figure S1B represent intersegment angles between adjacent body segments from head (segment angle 1) to tail (segment angle 24). Small gaps (up to 4 frames) in the depicted angles time series were interpolated using cubic interpolation. Angles were smoothed over 6 frames (i.e. 0.6 sec) for visualization.

Data presentation

For graphs displaying trial-averaged behavior data, the mean represents the mean across all tracks across all assays (typically ~100 animals per assay). For speed and reversal data, the standard error accounts for track-to-track variability. For graphs displaying fraction quiescent or head-waving, the mean represents the mean fraction across experiments and the standard error accounts for experiment-to-experiment variability. For visualization, speed and quiescence data are shown in 15 frames (= 5 seconds) bins and reversals are shown in 45 frames (= 15 seconds) bins. All intervals for behavior quantification were chosen to optimally reflect the behavior in question. For reversals, the interval of maximal change upon O₂ downshift is quantified; these time points were slightly different for each feeding state but consistent across genotypes. To display speed recovery, three time points needed to be quantified and set in relation to each other: basal speed (Speed_{max}, indicated by black bar in Figures 1B and S3A), minimum speed immediately following O₂ downshift (Speed_{min}, red bar in Figures 1B and S3A) and sustained speed towards the end of O₂ downshift (Speed_{sust}, cyan bar in Figures 1B and S3A). For calculation of speed recovery, the absolute sustained speed (Speed_{sust}) was normalized to a linear scale using the formula: $(\text{Speed}_{\text{sust}} - \text{Speed}_{\text{min}}) / (\text{Speed}_{\text{max}} - \text{Speed}_{\text{min}})$. For the quantification of quiescence and head-waving behavior, we quantify steady state levels, i.e. once they have established upon O₂ downshift.

All statistical analyses of behavioral data (Figures 1, 2, S1A, S1D, S1E, S1G, S2D, S3A and S3C-S3E) were performed to account for experiment-to-experiment variability, i.e. each data point used for generating bar graphs or box plots was a population average calculated from each individual experiment. Statistical tests were applied as described below under ‘Quantification and Statistical Analysis’.

State transition diagrams

For each active (A), head-waving (H) and quiescent (Q) state outbound rates of state transitions were calculated as per second probabilities. Behavioral states were determined in bins of 1 sec. For each track, the sum of events of every possible transition was calculated. From all active, head-waving and quiescent states 4 transition paths were possible (i.e. into the remaining two states, self-transition, and transition into an undefined state). Undefined states corresponded to time points at which active states were interrupted but the lengths of the detected bouts did not reach threshold values to be designated neither quiescent nor head-waving. Transition rates were calculated per experiment by summing all transition events of one kind (e.g. AA) and dividing by the total number of transition events from the same state of origin (e.g. AA + AH + AQ). Transitions into NaN were neglected.

Feeding quiescence

Individual starved worms were examined under a stereomicroscope for 60 sec. Quiescence during the observation period needed to last for at least 10 sec to be considered a quiescent episode. Worms during quiescent episodes (n = 20 worms, 28 quiescent episodes) were scored for pumping, as judged by movement of the terminal pharyngeal bulb. Worms that were quiescent for the entire 60 sec observation period were touched with a worm pick to confirm reversibility of quiescence. Scored worms were removed from the plate to avoid second examination. A total number of 3 pumps was counted across all worms and quiescent episodes. All pumps occurred during quiescence episodes that spanned the entire 60 sec observation period. 1 worm exhibited 2 pumps that occurred spaced by approximately 20 sec; the third pump occurred as a single event in a different worm.

Approximating worm posture by eccentricity

We used absolute eccentricity values in 1 sec bins for time points at which tracks were identified as either quiescent or active. Of the active time points, we only considered fast movement (speed > 0.1 mm/sec) and excluded time points at which the animal was found to engage in pirouette behavior (i.e. performing reversals or turns). This allowed to compare quiescent animals to their posture-wise most similar counterpart (i.e. worms that move rapidly forward by propagation of sinusoidal waves). Eccentricity was chosen to be displayed as $1 - \varepsilon$ to aid subsequent visualization. Eccentricity values were binned in increments of 0.005 and the cumulative sum of the binned data was calculated. Significance was determined by a customized resampling test in MATLAB. For each of the 28 experiments, eccentricity values for all bins were pooled and equal numbers of samples as originally observed were randomly drawn without replacements to obtain two test cumulative density functions (CDF), like for the original data shown in Figure S1C. Then we calculated the L₁ distance (i.e. absolute difference) between the 2 test CDFs. This resampling procedure was performed 10⁶ times for each experiment (n = 28) and p_n, which is the fraction of distances equal to or larger than the original one, was recorded for each of the n = 28 runs. The final p-value is the mean of p_{n(1-28)}.

Reversal probabilities of active and quiescent worms

For this analysis, the quiescent state was detected in 10 sec bins rather than sliding windows in order to obtain temporally precise boundaries. Worms that were either active or quiescent for 2 min prior to O₂ upshift and for which the track continued for at least 1 min following O₂ upshift were used. Reversals were calculated in 2 sec bins for each track and are shown as mean fraction of animals reversing across experiments.

Determination of behavioral state bouts and correlations

Bouts were extracted from tracks with a minimal track length of 1800 sec (median track length: 4682 sec) during the 10% O₂ period (earliest starting at minute 45) of the experiments shown in Figure 1F. The median length of behavioral state bouts was 40-70 sec but the distribution of all detected states (active, head-waving, quiescent) exhibited long-tailed distributions with bout lengths of up to 30 min, leading to a non-Gaussian distribution of the data. Only subsets of all detected bouts were used for correlation analyses (Figures S2E-S2H): we excluded bout pairs in which either the preceding bout started with the beginning of the track or the succeeding bout was interrupted by the track end, respectively, in order to ensure that our analysis only included complete bouts. Since quiescence periods were often directly preceded or followed by head-waving bouts, we allowed for a head-waving period of average length (60 sec) to separate active from succeeding quiescence bouts (and vice versa).

Axes cropping of scatter plots omitted data points, which were included in correlation analysis. Number of data points cropped: 3 (Figure S2E, S2F), 32 (Figure S2G), 6 (Figure S2H). Due to the non-normality of the underlying data, correlations and p-values were calculated using the Spearman rank correlation test in GraphPad Prism.

Pharyngeal pumping

WT and *daf-2(e1370)* mutant worms were shifted to 25°C in the evening before the experiment. Also in the evening before the experiment, thin NGM agarose pads (created by pouring melted agarose into a ring 2.45 mm thick and 50 mm in diameter and enclosed with glass on both sides to allow hardening into a smooth surface, as described previously (Kato et al., 2015)) were seeded with 50 µl of an *E. coli* OP50 overnight culture and kept at 37°C overnight. In the morning, the agarose pads were brought to the experiment room and allowed approximately 30 min to acclimate to the room temperature. Worms were kept at 25°C until used. Worms were placed on the agarose pad and allowed to adapt to the pad and room conditions for 15-25 min before the recording started. Prior to the recording, the agarose pad was placed inside an imaging chamber previously described for Ca²⁺ imaging in freely-moving worms (Kato et al., 2015) and covered with a 0.55 mm thick glass slide 0.7 mm from the agarose surface. The chamber containing the agarose pad was then placed onto a motorized stage with associated controller (MS-2000-PhotoTrack, Applied Scientific Instrumentation), allowing to follow the worm as it moved freely on the food lawn. Brightfield images were acquired for 4-4.5 min at an inverted compound microscope (Zeiss Axio Observer Z1) using an EMCCD camera (Evolve 512, Photometrics) and a 10x objective (Zeiss Plan-APOCHROMAT, NA 0.45) at 30 Hz using VisiView software (Visitron Systems GmbH, Germany). For each worm, pumping was counted as contractions of the terminal pharyngeal bulb for two 30 sec periods and each data point represents the average of both periods.

Determining overlap in expression pattern

The overlap in expression pattern between the *Pglr-4* and *Posm-9* promoter fragments was determined by taking z-stacks in a strain that was generated by crossing the *Posm-9::daf-2a::SL2::mCherry* rescue strain to a *Pglr-4::gfp* reporter line. Images were taken at an inverted spinning disk microscope (UltraViewVoX, PerkinElmer), equipped with an EMCCD camera (C9100-13, Hamamatsu). The overlap was determined by analyzing each z-plane individually using Fiji software and no coexpression of *gfp* and *mCherry* could be detected. *Posm-9* and *Pglr-4* are reported to overlap in their expression in FLP (Brockie et al., 2001; Colbert et al., 1997); however, we were unable to detect any overlap, suggesting lack of FLP expression under one of the promoters or expression below the detection limit.

Imaging of brain-wide neural activity in microfluidic chip

Imaging of brain-wide neural activity was done as described previously (Kato et al., 2015). Two-layer PDMS microfluidic devices were used to immobilize and stimulate worms (Schrödel et al., 2013; Zimmer et al., 2009). The worm channel was connected to a syringe containing 1 mM Tetramisole in NGM buffer. The microfluidic device was connected to the syringe using Tygon or polyethylene tubing. Worms were food-deprived on NGM agar plates as described for the worm population behavioral recordings. Illumination and piezo stage were started 2 min prior to image acquisition. Images were acquired at an inverted spinning disk microscope (UltraView VoX, PerkinElmer), equipped with an EMCCD camera (C9100-13, Hamamatsu). Images were acquired at 2 µm spacing over 12-15 z-planes, depending on the feeding state and, hence, size of the animal. These settings translated into an acquisition rate

of 1.6-2.6 volumes per second. Gas flow at a rate of 50 ml/min was achieved and controlled as described for the worm population behavioral recordings. The stimulus protocol used was identical to the behavioral paradigm (6min 21% O₂ – 6min 10% O₂ – 6min 21% O₂). All gas mixtures were balanced with N₂.

For each condition (WT fasted, WT starved, *daf-2* fasted), 6 datasets were generated from which neural traces of all detected neurons were extracted. These datasets were used for analyses on brain-wide changes and to perform principal component analysis (Figures 3A-3C, 4A, 5, 6A, 6B, 6D and S4). Furthermore, neural traces of spontaneously active sensory neurons (Figures 4B and 6E) were exclusively extracted from those datasets. To increase statistical power for some analyses, additional datasets were generated (in total: WT fasted = 10, WT starved = 11, *daf-2* fasted = 11) from which only neural traces of identifiable neurons were extracted, which include all neurons used to classify quiescent versus active brain states; these data in combination with the complete datasets were used for Figures 3D, 3E, 4C, 6C, 6F, 7, S5, S6 and S7. For datasets of WT starved at constant 21% O₂, only traces of neuronal classes required to determine the brain state were extracted (Figure 3E).

Neural time series extraction

Tracking and analysis of brain-wide imaging recordings was done as described previously (Kato et al., 2015), using custom MATLAB scripts. Briefly, ROIs were detected as local maxima in a noise- and motion-corrected reference ROI movie using a thresholding approach. The reference movie was generated by averaging successive blocks of movie frames. The number of averaged frames was chosen depending on the degree of movement in the recording and ranged from 40-100. ROIs in adjacent reference movie frames were joined based on closest distance relative to global inter-frame motion, thereby creating time-varying ROIs. ROIs present in adjacent z-planes were joined to create one spacetime voxel set. The adjoining process of all detected ROIs was proof-checked manually, falsely joined or created ROIs removed if necessary, and neurons that remained undetected during the automatic process were added manually.

Neuronal traces were extracted as z-plane-specific background-subtracted fluorescence intensity maxima at every time point. $\Delta F/F_0$ as calculated here uses the mean fluorescence intensity across a trial for each neuron as F_0 . For BAG and URX O₂-sensory neurons (Figures 7A-7D and S7), which have lowest calcium at 21% and 10% O₂, respectively, $\Delta F/F_0$ was recalculated using the lowest 20% of fluorescence intensity values during a 60 sec period at 21% (BAG: 730-790 sec into recording) and 10% O₂ (URX: 370-430 sec into recording), respectively. All neural traces used here were de-trended to account for fluorophore bleaching.

Identification of head ganglia neurons

Between 114 and 149 neurons were detected in the head ganglia region of each WT recording, corresponding to 58%-76% of expected neurons. The number of detected neurons was slightly lower in *daf-2* animals (103-117 neurons, i.e. 53%-60%) due to the longer body size of *daf-2* mutants and thus fewer neurons in the field of view. Identification of neurons was based on their position relative to other neurons as well as their activity pattern (Kato et al., 2015). We confirmed the identity of ASK using the *Psrbc-64* marker (Kim et al., 2009). Some neuron identities remained ambiguous; these neuron classes are denoted with ‘ ϕ ’ and alternative identities are listed in brackets here: URA (URY, IL1), URY (URA, IL1).

Trace state annotation by segmentation

Neural time series were segmented into rise – high – fall – low phases as described previously (Kato et al., 2015). In brief, rise and fall phases of neurons were assigned when the time derivatives of $\Delta F/F_0$ traces were above and below a threshold of 5% of a neuron’s full dynamic range, respectively. High and low phases were assigned to the in-between periods when $\Delta F/F_0$ remained at high or low values respectively, leading to the phase order rise – high – fall – low or rise – fall – low for some neurons (e.g. SMD or RIV). The global motor command state (forward – reverse – turn (dorsal or ventral)) corresponds to the low – rise + high – fall phases of AVA.

Brain state determination

Active and quiescent brain states were determined as described previously (Nichols et al., 2017). Briefly, quiescent brain states were defined by the absence of activity across 4 neuronal classes that unambiguously define motor behavior in freely behaving animals (Kato et al., 2015): fall and low phases in AVA, VB01 or VB02, SMDV, RIV and SMDD. Quiescence periods in Figures 3D, 3E and 6C were quantified as fraction of time spent in the quiescent brain state in 1 min bins.

Principal component analysis

Principal component analysis (PCA) was performed as described previously (Kato et al., 2015), with some modifications. Total-variation regularization (Chartrand, 2011) was used to compute de-noised time derivatives of $\Delta F/F_0$ neural traces. Each trace was normalized by the peak magnitude of their non-derivative $\Delta F/F_0$ time series. O_2 -sensory, AVF and ASK neurons were excluded from the analysis, as were neurons that showed sudden strong, uncorrelated and nonrecurring activity. For generating phase plots, all neuronal time series data were projected onto the first 3 eigenvectors (in 2 cases (Figure S4B), we chose eigenvector 4 instead of 3 when SMDD neurons had their maximal weight in eigenvector 4 instead of 3). These projections represent the time series of the latent variables and were termed principal components (PCs). Temporal PCs are the time integrals of PCs. The quiescent brain state in PCA space is not merely at zero but is offset by the activity of sleep-active neurons like the RMEs and RIS, which have a high weight on the first 3 eigenvectors. Phase plot trajectories are smoothed using a 3-sample sliding-average filter for visualization purposes.

Percentage of total variance explained

For comparing the percentage of total variance explained by each principal component (Figure 5C), we performed PCA as described above but restricted to the time periods that were determined active, thus sparing the quiescent time periods. We calculated the cumulative variance explained for the first 10 PCs from this analysis. Significance was determined using a resampling approach in MATLAB. We systemically resampled, without replacements, all possible combinations of pairs of datasets that can be drawn from a total of 12 recordings (n=6 for each WT fasted and WT starved), resulting in 461 possible combinations, excluding the actual dataset combination. We then calculated the mean cumulative frequency distributions for each group of resampled datasets and the L_1 distance (i.e. difference in the area under the curve (dAUC)) between them. The p-value indicates the fraction of combinations that resulted in a dAUC greater or equal to the difference between the experimental mean distributions.

Determining a neuron's principal active state

This was done as described previously (Nichols et al., 2017). Many neurons are known to be specifically active during either forward or reverse brain states. To determine each neuron's principal active state, we split the active brain state into reverse (when AVA was rising or high) and forward (when AVA was falling or low) brain states. The determination of the principal active state was done based on the distribution of $\Delta F/F_0$ during reverse and forward/turning states. Many neurons show high activity during one and low activity during the other state and were classified accordingly. Neurons with comparably high $\Delta F/F_0$ during both reverse and forward/turn states were classified as indiscriminative.

Mean activity distribution

For analysis of global neural activity (Figures 4A, 5D and 6D), all segmented neurons were included, except for neurons that responded to O_2 stimulation (BAG, URX, AQR, IL2). Dashed grey lines in Figures 4A and 6D indicate an inactivity cutoff: Manual inspection of all individual neural traces led to the conclusion that signals in neuronal time series with a mean $\Delta F/F_0$ value < 0.2 cannot clearly be distinguished from noise. To determine the cumulative frequency distributions of $\Delta F/F_0$ means for active and quiescent periods separately, composite traces were built that, for each neuron, consisted of all frames at either active or quiescent time points. The mean of each composite trace was calculated and these values were sorted and binned in increments of 0.06, resulting in 24 bins, and divided by the total number of data points to estimate the probability density function (PDF). We then calculated the cumulative sum of the PDF of each dataset separately; shown are the means (\pm SEM) across all datasets.

Calculation of mean $\Delta F/F_0$ for selected neurons (Figures 4C, 6F and S6A-S6C) was done by calculating the mean for composite traces of active and quiescent time periods for selected neurons. The respective active state for each neuron was defined by its principal state (see 'Determining a neuron's principal active state'). Data are presented as sorted from highest to lowest mean $\Delta F/F_0$ during the respective active state.

Calculation of mean $\Delta F/F_0$ of sensory neurons (Figures 4B and 6E) was performed as described for global $\Delta F/F_0$ calculations. Putative sensory neurons were assigned based on their position in the anterior region of the lateral ganglion, in which a majority of amphid sensory neurons are located (www.wormatlas.org). The most dorsal neuron included in the analysis was the unambiguously identified ASK neuron. The putative sensory neurons showed spontaneous activity that occurred largely uncorrelated with the global motor command state. The identification of most sensory neurons remained ambiguous.

Significance of active global mean distributions (Figure 5D) was determined as described above for 'Percentage of total variance explained'. We systemically resampled, without replacements, all possible combinations of pairs of

datasets that can be drawn from a total of 12 recordings ($n=6$ for each WT fasted and WT starved), resulting in 461 possible combinations, excluding the actual dataset combination. We then calculated the mean cumulative frequency distributions for each group of resampled datasets and the L_1 distance (i.e. difference in the area under the curve (dAUC)) between them. The p-value indicates the fraction of combinations that resulted in a dAUC greater or equal to the difference between the actual mean distributions. Significances of global mean distributions between active and quiescent periods (Figures 4A, 4B, 6D and 6E) were determined using a permutation test in MATLAB, by randomly placing quiescent blocks on each recording while maintaining the lengths of the original quiescent blocks to obtain two test cumulative distribution functions (CDFs), as for the original ones. This procedure was repeated 10^6 times for each dataset. For each iteration, we calculated the L_1 distance (i.e. absolute difference) between the two reshuffled CDFs. The p-value indicates the fraction of all iterations that resulted in a difference between 2 randomly reshuffled distributions at least as large as the original one.

RIS activity distribution

The graphs in Figure S6D display the distributions of all $\Delta F/F_0$ values for RIS during its principal active state (i.e. forward/turn) from all datasets in which RIS could be detected (WT fasted = 9, WT starved = 11, *daf-2* fasted = 10). For each genotype/condition, the histograms display the fraction of frames in which the logarithmically binned $\Delta F/F_0$ values were observed. Significance was determined by a custom resampling test in MATLAB. For each pairwise comparison, all forward/turn bout periods were pooled and the same number of bouts as originally observed for each genotype/condition were randomly re-assigned without replacements to calculate two test distributions. This procedure was repeated 10^6 times. For each iteration, we calculated the L_1 -distance (i.e. the absolute difference) between the two resampled distributions. The p-value was calculated as the fraction of all iterations that resulted in a distance at least as large as the one measured between the original distributions. They were adjusted using the Bonferroni correction, i.e. by multiplying by the number of total pairwise comparisons performed.

Quantification of evoked responses in O₂-sensory neurons

Quantification of peak and sustained responses in BAG and URX sensory neurons was done by calculating, for each trace, the average $\Delta F/F_0$ over a 1-2 sec (peak) and 5 sec (sustainedness) interval of $\Delta F/F_0$ neural traces. As the time point of peak activity in URX neurons was variable the interval to quantify was individually determined for each trace (see also Figure S7).

ASK peak analysis

ASK peaks and corresponding amplitudes were detected as local maxima in $\Delta F/F_0$ ASK neural traces. Detected peaks were attributed to the quiescent or active brain state episodes according to their occurrence in time. Data are presented as mean amplitude per neuron.

Quantification and Statistical Analysis

For WT starved animals in the short-term experiments 28 experiments were performed in total. Figures S2C and S2D contain data from all these experiments while WT starved data used to generate Figures 1A-1D, S1A, S1D-S1E and S1F are subsets of these data, which are the WT control experiments performed in parallel to the other conditions. These overlapping data were usually not used in several panels. 3 data points occur in more than one of these figure panels because these experiments were performed as controls, and these exceptions are as follows: Figures S1D, S1E and S1F share three data point with Figures 1A-1D and one data point with Figure S1A. Note that Figures S1D, S1E, S1F show quantifications of different behaviors/time points from the same experiments. WT starved data used as controls for *daf-2* experiments (Figures 2A, 2B, S3A and S3C) represent an individual dataset for which animals were treated as their temperature-sensitive *daf-2* counterparts, as described in ‘Worm population behavioral recordings’. Most statistical tests were performed in GraphPad Prism 7, all resampling tests were performed using custom scripts in MATLAB. Details on the statistical test as well as exact details on sample size, displayed data and p-values can be found with each figure legend. In most cases, parametric statistical tests were used. If the n-number > 8, a D’Agostino-Pearson omnibus K2 test was performed in GraphPad Prism to test for normality. Subsequent test decisions were based on this. If more than 2 groups were compared, appropriate post-tests were performed. See also individual figure legends, which denote the respective post-test used. The individual method sections contain information on statistics when resampling tests were used. For tests performed in GraphPad Prism, a significance level of 0.05 was used. The experimenters were not blinded to the experimental conditions.

Raw data, worm strains, molecular biology constructs and MATLAB code are available upon request.

Supplemental References

Brockie, P.J., Madsen, D.M., Zheng, Y., Mellem, J., Maricq, A.V. (2001). Differential expression of glutamate receptor subunits in the nervous system of *Caenorhabditis elegans* and their regulation by the homeodomain protein UNC-42. *J. Neurosci.* *21*, 1510-1522.

Chartrand, R. (2011). Numerical differentiation of noisy, nonsmooth data. *ISRN Applied Mathematics* *2011*, 1-11.

Chelur, D.S., Chalfie, M. (2007). Targeted cell killing by reconstituted caspases. *Proc. Natl. Acad. Sci. U.S.A.* *104*, 2283-2288.

Hung, W.L., Wang, Y., Chitturi, J., Zhen, M. (2014). A *Caenorhabditis elegans* developmental decision requires insulin signaling-mediated neuron-intestine communication. *Development* *141*, 1767-1779.

Jansen, G., Thissjen, K.L., Werner, P., van der Horst, M., Hazendonk, E., Plasterk, R.H. (1999). The complete family of genes encoding G proteins of *Caenorhabditis elegans*. *Nat. Genet.* *21*, 414-419.

Kim, K., Sato, K., Shibuya, M., Zeiger, D.M., Butcher, R.A., Ragains, J.R., Clardy, J., Touhara, K., Sengupta, P. (2009). Two chemoreceptors mediate developmental effects of dauer pheromone in *C. elegans*. *Science* *326*, 994-998.

Mano, I., Straud, S., Driscoll, M. (2007). *Caenorhabditis elegans* glutamate transporters influence synaptic function and behavior at sites distant from the synapse. *J. Biol. Chem.* *282*, 34412-34419.

Nonet, M.L., Staunton, J.E., Kilgard, M.P., Fergestad, T., Hartweg, E., Horvitz, H.R., Jorgensen, E.M., Meyer, B.J. (1997). *Caenorhabditis elegans* rab-3 mutant synapses exhibit impaired function and are partially depleted of vesicles. *J. Neurosci.* *17*, 8061-8073.

Ohno, H., Kato, S., Naito, Y., Kunitomo, H., Tomioka, M., Iino, Y. (2014). Role of synaptic phosphatidylinositol 3-kinase in a behavioral learning response in *C. elegans*. *Science* *345*, 313-317.